RESONANT FREQUENCY TUNING OF A NONLINEAR HELICOPTER INCEPTOR MODEL: A SENSITIVITY ANALYSIS

Edward J. H. Yap, D.Rezgui, M.H.Lowenberg, S.A.Neild

Department of Aerospace Engineering,

University of Bristol, Queens Building, Bristol, BS8 1TR, UK

Khosru Rahman

BAE Systems, Rochester, Kent, ME1 2XX, UK

ABSTRACT

The term inceptor refers to the controls pilots use to orientate and manoeuvre an aircraft, applicable to both fixed or rotary-wing aircraft. Active inceptors are unique in that they include the ability to provide tactile force feedback from the aircraft control surfaces to the pilot; the pilot is able to experience the aircraft dynamics. Typical active inceptor anatomies comprise components interconnected through a network of mechanical links and understanding how these individual components behave collectively under the influence of helicopter vibratory loads is crucial in assessing the dynamic response of the entire inceptor. This paper presents an investigation into the mathematical modelling of a candidate inceptor mechanism using a dynamic modelling approach formulated by Udwadia-Kalaba to explore resonance frequencies. Results demonstrate the ability of the Udwadia-Kalaba scheme to model and capture the location of the inceptor mechanism's resonance frequencies. Sensitivity studies were also conducted on selected inceptor design parameters to demonstrate that system resonance frequencies may be influenced and tuned away from baseline values.

1. INTRODUCTION

Inceptors, whilst commonly referred to as 'sticks', incorporate a whole class of pilot interface controls ranging from centre sticks, side sticks, cyclics, collectives and throttles. Active inceptors include the additional ability to provide tactile force feedback from the aircraft control surfaces to the pilot. Whilst typically reserved for military applications[1], there has been a gradual shift in focus to integrate active inceptors within the civilian aviation sector fuelled by some notable high profile events[2].

However, current research trends on aircraft active inceptors for fly-by-wire systems have focused predominantly on fixed wing aircraft and as such there is a relative lack of research and guidance associated with active inceptors for rotorcraft applications[3]. Underlying rotorcraft phenomena such as Rotorcraft Pilot Couplings (RPCs) and pilot Biodynamic Feedthrough (BDFT)[4,5] may introduce adverse and undesired destabilizing aircraft vibrations and are examples of adverse associations that exist between rotorcraft and their vibrations which continues to be an active field of research[6].

Typical active inceptor anatomies utilise combinations of linear and torsional springs, servo actuators, motors, spherical bearings, ball bearings and displacement and force transducers[8]. These are all interconnected through a network of mechanical links and as illustrated in the block schematic in Figure 2. Understanding how these individual components behave collectively when under the influence of helicopter vibratory loads is crucial in assessing the dynamic response of the entire inceptor unit and maintaining the performance levels required throughout its service life. Rotary vibratory loads are considered the key driver when designing for vibrations within a helicopter[9] and some inceptor system resonances may well occur at or near the

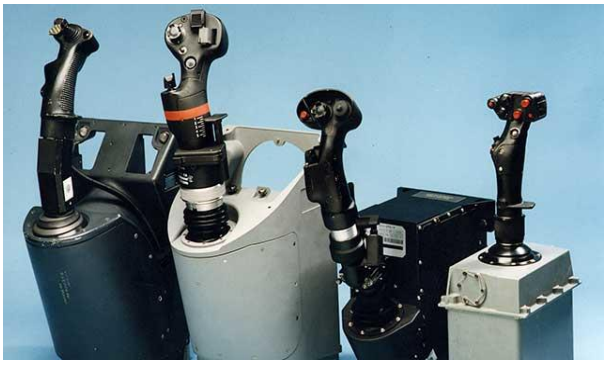

Figure 1: Aircraft inceptor control systems[7]

Presented at 45th European Rotorcraft Forum, Warsaw, Poland, 17-20 September, 2019

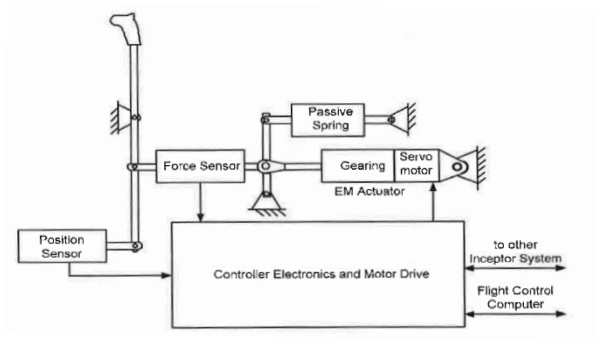

Figure 2: Active Inceptor functional diagram[8]

aircraft's forcing frequencies and it is imperative that this is avoided.

Figure 2 depicts the general functional requirements and anatomy of a typical active inceptor system detailing the connections between servo actuation, electronic controller, spring assembly and force sensor sub systems[8].

In early industrial design stages, the dynamic characteristics and performance of an active inceptor may not be adequately assessed nor predicted; the inceptor design is said to be in a continual state of change and the use of finite element analysis to assess the dynamic behaviour of the full system may not be efficient or even appropriate until the detailed design stage. This limitation can present a challenge if significant issues emerge once the inceptor design is finalised, such as system component resonances occurring at or close to the aircraft's forcing frequencies dominated by rotating components such as the main or tail rotor as specified by the MIL-STD-810G[9] and as illustrated schematically in Figure 3.

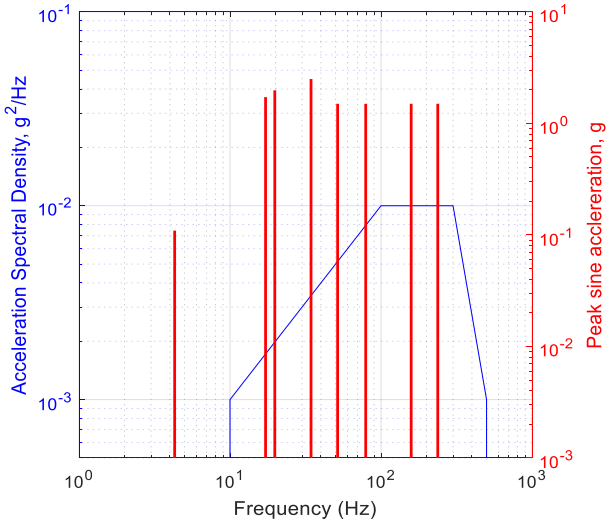

Figure 3: 'Sine on Random' vibration profile for a UH-60 Helicopter. Level information extracted from MIL-STD Category 14 Method 514.6[9]

Additional iterations in the design cycle may lead to a shift of inceptor component resonances to now occur near the aforementioned forcing frequencies. Coupled with the requirement to completely rebuild or update models and the adverse impact on industrial project time scales, there is a general reluctance within industry to modify an inceptor design upon its finalisation.

The drawbacks of this current design approach motivate the need to develop an efficiently configurable mathematical model of a candidate active inceptor. The development of a mathematical model of an active inceptor would provide an early low-cost means of predicting the dynamics of the inceptor mechanism in the preliminary design stage. The occurrence of adverse vibration issues may be pre-empted through frequency response analyses and, by conducting sensitivity study investigations on system design parameters, inceptor resonant frequencies may be identified and tuned to arrive at acceptable design configurations that comply with specified frequency restrictions. The intention being that this process would aid and inform conceptions of Computer Aided Designs (CAD), Finite Element (FE) models and experimental units in the detailed design phase.

Figure 3 illustrates a vibration profile termed 'Sine on Random'. Sine on Random refers to a specific class of vibration profiles designed for the purpose of vibration testing of helicopter internally stored cargo as outlined within MIL-STD Category 9 Method 514.6[9]. The intention is to simulate the worst-case environments the component may be subjected to throughout its lifetime. Sine on Random profiles are helicopter specific as illustrated in Figure 3 for the UH-60 helicopter.

Sine on Random vibration profiles are unique in that they comprise strong narrowband peaks of sinusoidal vibration provided by the helicopter's rotating components (predominantly driven by the main rotor and tail rotor) superimposed over a wideband low-level random vibration due to aerodynamic flow.

Requirements stipulate a duration of 12 hours for such vibration testing, which will provide an equivalent effective representation of 2500 operational hours.

The nature of the inceptor involving components characterized by kinematic non-linearity that can endure significant displacements highlights the importance of investigating Multi-Body Dynamic (MBD) modelling approaches if an accurate mathematical representation model of the inceptor mechanism system is to be developed.

The contribution of this paper is the application of the dynamic modelling approach formulated by Udwadia-

Presented at 45th European Rotorcraft Forum, Warsaw, Poland, 17-20 September, 2019

Kalaba[10] for use in this work to model a candidate inceptor mechanism system such that system resonances may be explored and tuned through sensitivity analyses of design parameters. The Udwadia-Kalaba approach is proposed due to its handling of mechanical systems subjected to kinematical constraints, its applicability to a wide class of constraints[10] and ability to provide explicit equation of motions without the use of Lagrange multipliers[11].

The following section provides a brief summary of the Udwadia-Kalaba dynamic modelling approach and description of terminologies adopted. Section 3 presents an application study of the Udwadia-Kalaba dynamic modelling approach on a test case study model prior to application on the inceptor which is presented in Section 4.

2. THE UDWADIA-KALABA DYNAMIC MODELLING SCHEME

The Udwadia-Kalaba[10] equation of motion as formulated in Eq.(1) tackles the issue of multibody mechanical systems subjected to kinematical constraints by reducing the system to a corresponding system of particles with the system's physical geometric constraints included as a separate entity. The equation of motion formulated by Udwadia-Kalaba is often referred to as 'The Fundamental Equation'.

$$\ddot{\mathbf{x}} = \mathbf{a} + \boldsymbol{M}^{-\frac{1}{2}}\left(\boldsymbol{A}\boldsymbol{M}^{-\frac{1}{2}}\right)^{+}(\boldsymbol{b} - \boldsymbol{A}\mathbf{a}) \quad (1)$$

$\ddot{\mathbf{x}}$ refers to the vector of true accelerations of the multibody system under the influence of its geometric constraints relative to the global reference frame.

$\mathbf{a}$ is the vector of accelerations of the multibody system in question due to the influence of impressed forces acting upon it. This term $\mathbf{a}$ is often referred to as the vector of accelerations of the unconstrained system. The size of this vector is $(q \text{ x } 1)$ with q denoting the number of system state variables.

$\boldsymbol{M}$ is the mass/inertia matrix of the system, size $(q \text{ x } q)$

$+$ is the Moore-Penrose generalized pseudoinverse function[12].

The Udwadia-Kalaba approach assumes that the set of constraint equations obtained for any generic system when differentiated twice with respect with time will yield a set of constraint equations that can be expressed as linear equality relations regarding accelerations between the particles of the system as in Eq.(2)

$$\boldsymbol{A}\ddot{\mathbf{x}} = \boldsymbol{b} \quad (2)$$

$\boldsymbol{A}$ is a $(p \text{ x } q)$ matrix obtained from differentiating the system's geometric constraint equations twice with respect to time and expressed in the form of (2). The quantity p denotes the number of independent geometric constraint equations associated with the system and terms within the matrix $\boldsymbol{A}$ consist of those associated with state accelerations.

$\boldsymbol{b}$ is a $(p \text{ x } 1)$ vector of terms not associated with state accelerations when the constraint equations are differentiated twice with respect to time.

The combined right hand side terms in Eq.(1) consisting of $\boldsymbol{M}^{-\frac{1}{2}}\left(\boldsymbol{A}\boldsymbol{M}^{-\frac{1}{2}}\right)^{+}(\mathbf{b} - \boldsymbol{A}\mathbf{a})$ effectively represent the additional accelerations and subsequent additional forces required to ensure the system complies with any kinematical constraint that it is subjected to.

This dynamic formulation approach has been investigated by Nielson *et al* [13], Li *et al* [14] and Pennestri *et al* [15] who all found convincing agreement of simulated system dynamic results with reference data.

3. MODEL TEST CASE: THE OVERCENTRE MECHANISM

Initial investigations into this MBD modelling approach firstly considered a test case study model system in order to provide an application study of the Udwadia-Kalaba dynamic modelling approach prior to application on the inceptor. The Overcentre Mechanism (Figure 4) was chosen as the test case model due to its basic, albeit crude, geometric

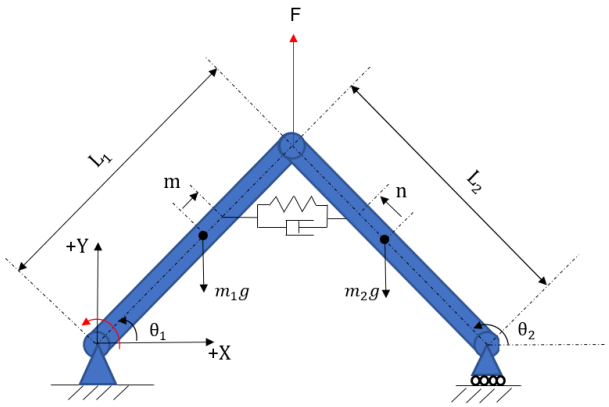

Figure 4: The Overcentre Mechanism

Presented at 45th European Rotorcraft Forum, Warsaw, Poland, 17-20 September, 2019

parallels with that of an inceptor involving linkages connected through joints.

This mechanism has also been studied previously by Knowles[16] including its nonlinear characteristics thereby providing a case study for which some results could be compared. This section details investigative studies associated with the Overcentre Mechanism and provides a formulative description of the Udwadia-Kalaba modelling process applied to this test model system.

The Overcentre Mechanism is a planar mechanism involving two rigid bars (denoted bar 1 and bar 2 in accordance with the notation in Figure 4) connected through a revolute joint. One end of bar 1 is attached to the ground through a revolute joint whilst the end of bar 2 is attached to the ground through a translational/revolute joint to allow for translational displacement. Bars 1 and 2 are connected via a revolute joint at their connection and a spring-dashpot attached between the two rigid bars provides means of translational resistance and energy dissipation. An external force (F) is chosen to be applied vertically at the connection between bars 1 and 2 although this point of application is not limited.

Table 1: Overcentre Mechanism parameter values

Parameters	Units	Value
L_1	metres	$2\sqrt{2}$
L_2	metres	$2\sqrt{2}$
m_1	kg	1
m_2	kg	1
m	metres	0
n	metres	0
Spring stiffness, k	Nm^{-1}	50
Dashpot damping coefficient, c	Nsm^{-1}	5

The mechanism is defined by six geometric position states (x_1, y_1, θ_1, x_2, y_2, θ_2 where θ_i represents bar rotations relative to the horizontal and x_i, y_i denote bar centre of gravity translations). Table 1 presents a brief summary of model parameters. The Udwadia-Kalaba dynamic modelling scheme places heavy emphasis on the accurate derivation of the system's geometric constraint equations. For the overcentre mechanism these are presented below through Eqs. (3) to (7). In order to compare the dynamic behaviour results of the Overcentre Mechanism from the Udwadia-Kalaba dynamic model, which is referred to as model 1, two other models were created. These are:

(3) $$x_1 - \frac{L_1}{2}\cos(\theta_1) = 0$$

(4) $$y_1 - \frac{L_1}{2}\sin(\theta_1) = 0$$

(5) $$x_1 + \frac{L_1}{2}\cos(\theta_1) - x_2 - \frac{L_2}{2}\cos(\theta_2) = 0$$

(6) $$y_1 + \frac{L_1}{2}\sin(\theta_1) - y_2 - \frac{L_2}{2}\sin(\theta_2) = 0$$

(7) $$y_2 - \frac{L_2}{2}\sin(\theta_2) = 0$$

Model 2: MATLABs Simscape MBD toolkit[17] model (Figure 5).

Model 3: A reduced order model modelled through the Lagrange formulations

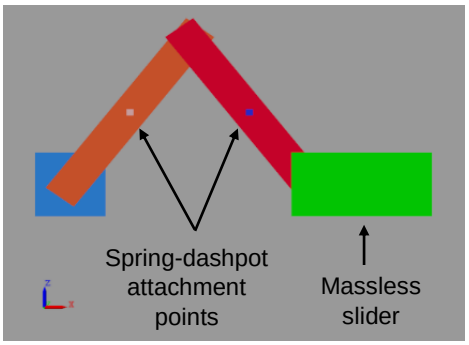

(a)

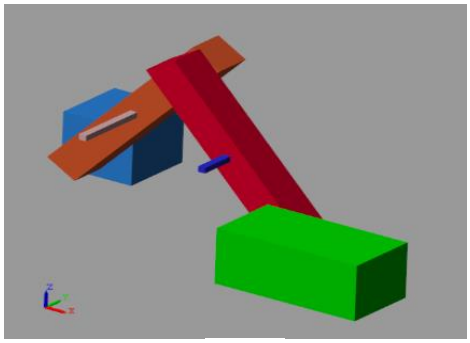

(b)

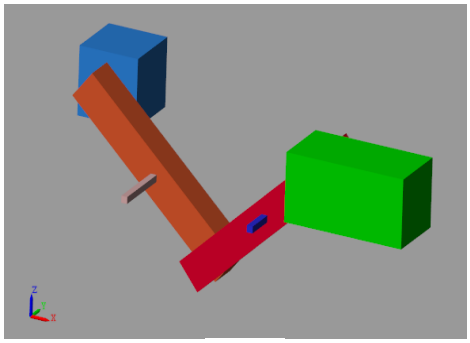

(c)

Figure 5: (a),(b),(c), MATLAB Simscape MBD model representation of the Overcentre Mechanism.

Presented at 45th European Rotorcraft Forum, Warsaw, Poland, 17-20 September, 2019

Considering equations (3) to (7), it may be observed that the specification of a single state variable would be sufficient in providing a full description of the overcentre mechanism's position and orientation. This is the basis of Model 3, a reduced order mathematical model dependent only on state θ_1, and modelled through the Lagrange equations of motion.

3.1 Static Model

Validation of the derived geometric constraint equations was performed through modelling the system's static responses using MATLAB's in-built FSOLVE function (version 2017a) and comparing responses with the dynamic Simscape MBD model.

External constant forcing of varying magnitude was applied vertically at the connection between bars 1 and 2 as in Figure 4. This external forcing was chosen to be the variable parameter and thus the static analysis conducted using MATLAB, formulated from the system's geometric constraint equations, required an additional static moment equilibrium equation as in Eq.(8)

$$(8)\quad \mathrm{Fsx}_1 * \left[\left(\frac{1}{2}-\frac{\mathrm{m}}{\mathrm{L}_1}\right) * \tan(\theta_1) - \left(\frac{1}{2}-\frac{\mathrm{n}}{\mathrm{L}_2}\right) * \tan(\theta_2)\right] + \mathrm{Fsy}_1 * \left[\frac{\mathrm{m}}{\mathrm{L}_1}-\frac{\mathrm{n}}{\mathrm{L}_2}\right] + \frac{1}{2} * (\mathrm{w}_1+\mathrm{w}_2) + \mathrm{F} = 0$$

The terms w_1 and w_2 denote the weight of bars 1 and 2. The terms Fsx_1 and Fsy_1 refer to spring-dashpot reaction forces associated with bar 1 in the global X and Y directions as in Figure 4. Considering the baseline system with parameters outlined in Table 1, Fsy_1 has a value of 0 and the expression for Fsx_1 is as follows.

$$(9)\quad \mathrm{Fsx}_1 = -[\mathrm{k} * (\mathrm{x}_1 - \mathrm{x}_2 + \mathrm{L}_0) + \mathrm{c} * (\dot{\mathrm{x}}_1 - \dot{\mathrm{x}}_2)]$$

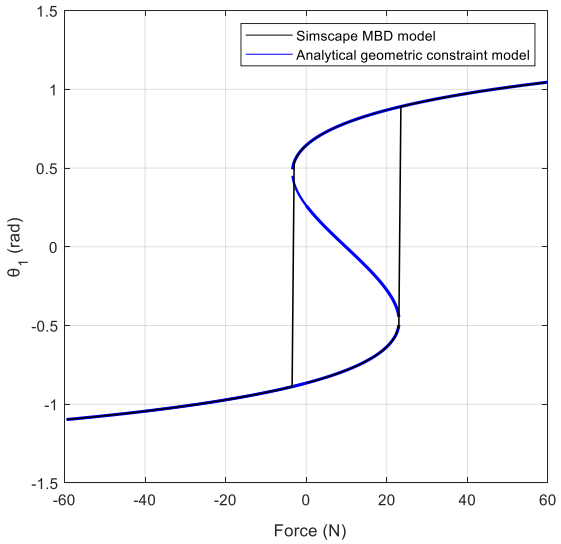

Figure 6: Overcentre Mechanism static response to a steady force application with varying magnitude.

L_0 is the natural unstretched length of the spring. Terms associated with velocity $(\dot{x}_1, \dot{x}_2)$ are ignored within the static model.

Results in Figure 6 from the static analysis of the Overcentre Mechanism show a strong agreement between the model formulated from the systems geometric constraint equations and that produced from the dynamic Simscape MBD model.

3.2 Dynamic Model

Effectively validating the derived system geometric constraint equations, the dynamic model of the mechanism was formulated within MATLAB based on the Udwadia-Kalaba dynamic approach. In accordance with the process outlined in section 2, the required matrices were derived as presented in Eqs.(10) to (13).

$$(10)\quad A = \begin{bmatrix} 1 & 0 & \frac{\mathrm{L}_1}{2}\sin(\theta_1) & 0 & 0 & 0 \\ 0 & 1 & -\frac{\mathrm{L}_1}{2}\cos(\theta_1) & 0 & 0 & 0 \\ 1 & 0 & -\frac{\mathrm{L}_1}{2}\sin(\theta_1) & -1 & 0 & \frac{\mathrm{L}_2}{2}\sin(\theta_2) \\ 0 & 1 & \frac{\mathrm{L}_1}{2}\cos(\theta_1) & 0 & -1 & -\frac{\mathrm{L}_2}{2}\cos(\theta_2) \\ 0 & 0 & 0 & 0 & 1 & -\frac{\mathrm{L}_2}{2}\cos(\theta_2) \end{bmatrix}$$

$$(11)\quad b = \begin{bmatrix} -\frac{\mathrm{L}_1}{2}\dot{\theta}_1^2\cos(\theta_1) \\ -\frac{\mathrm{L}_1}{2}\dot{\theta}_1^2\sin(\theta_1) \\ \frac{\mathrm{L}_1}{2}\dot{\theta}_1^2\cos(\theta_1) - \frac{\mathrm{L}_2}{2}\dot{\theta}_2^2\cos(\theta_2) \\ \frac{\mathrm{L}_1}{2}\dot{\theta}_1^2\sin(\theta_1) - \frac{\mathrm{L}_2}{2}\dot{\theta}_2^2\sin(\theta_2) \\ -\frac{\mathrm{L}_2}{2}\dot{\theta}_2^2\sin(\theta_2) \end{bmatrix}$$

$$(12)\quad M = \begin{bmatrix} m_1 & 0 & 0 & 0 & 0 & 0 \\ 0 & m_1 & 0 & 0 & 0 & 0 \\ 0 & 0 & \mathrm{I}_1 & 0 & 0 & 0 \\ 0 & 0 & 0 & m_2 & 0 & 0 \\ 0 & 0 & 0 & 0 & m_2 & 0 \\ 0 & 0 & 0 & 0 & 0 & \mathrm{I}_2 \end{bmatrix}$$

I_1 and I_2 are the inertia terms of bars 1 and 2, taken about their C.G locations and in the axis about which they rotate (Z-axis).

$$(13)\quad \mathrm{a} = \begin{bmatrix} a_{spring} \\ -g \\ 0 \\ a_{spring} \\ -g \\ 0 \end{bmatrix}$$

Presented at 45th European Rotorcraft Forum, Warsaw, Poland, 17-20 September, 2019

The accelerations due to gravity (g) and action of the spring-dashpot restoring forces (a_{spring}) are considered in Eq.(13), the vector of accelerations of the unconstrained system.

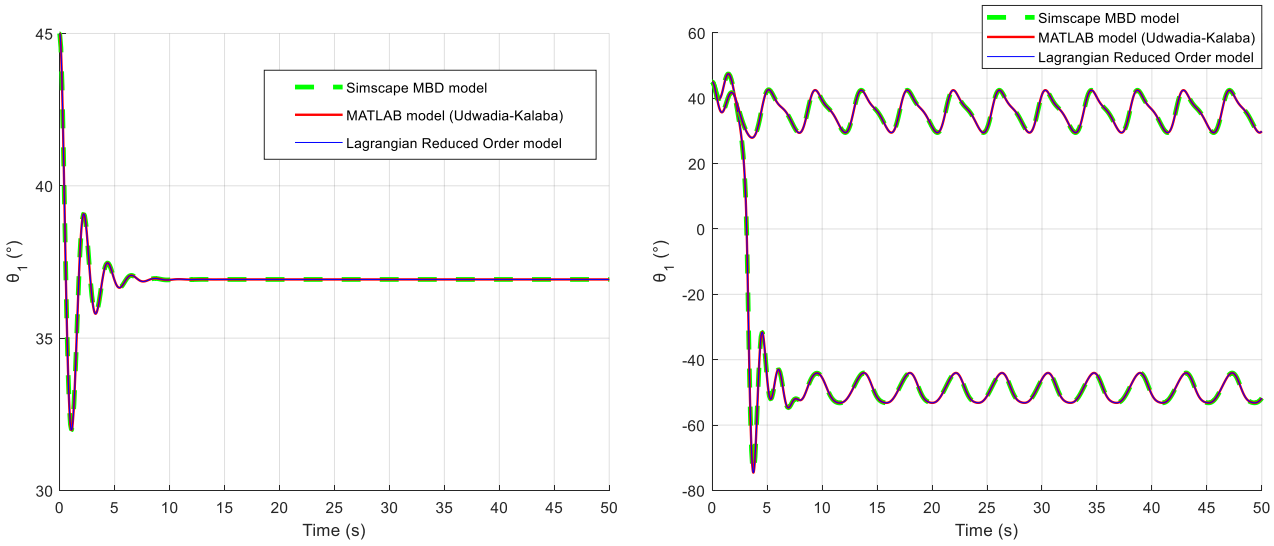

Figure 7: Baseline Overcentre Mechanism a) Free dynamic response (forcing amplitude, F0=0N), b) Dynamic response of the mechanism when subjected to two sinusoidal forces (forcing frequency, ω: 1.5 rads^{-1}, forcing amplitudes, F0= 3N and 10N).

The dynamic modelling of this mechanism was formulated within MATLAB based on the Udwadia-Kalaba approach. Models 2 and 3 (Simscape MBD and Lagrangian) were used to verify the system dynamic responses obtained from the Udwadia-Kalaba method through time history simulations.

Comparative studies were also carried out on configurations of the overcentre mechanism that deviated from geometric symmetry. These included combinations of the spring-dashpot being orientated arbitrarily, differing linkage lengths and arbitrary force application locations along the mechanism.

A Frequency Response (FR) analysis was also conducted on the baseline Overcentre Mechanism configuration defined in Table 1 to explore the location of the mechanism's theoretical natural frequency (1-Degree of Freedom, DoF). For this analysis the reduced order model modelled using the Lagrange formulations was considered and a sinusoidal force in the form F=F0sin(ωt) prescribed vertically at the bar connections as in Figure 4 to provide the excitation.

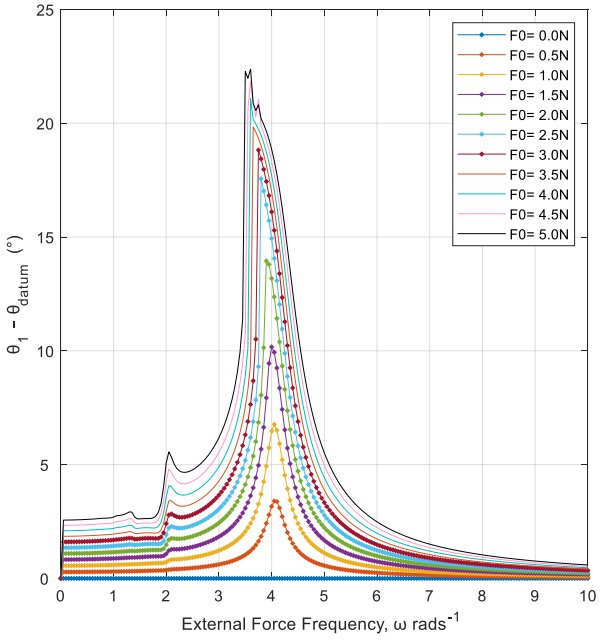

Figure 8: Frequency Responses (FR's) of the Overcentre Mechanism when subjected to a sinusoidal force of increasing forcing amplitudes (F0). Damping coefficient: 1 Nsm^{-1}.

Presented at 45th European Rotorcraft Forum, Warsaw, Poland, 17-20 September, 2019

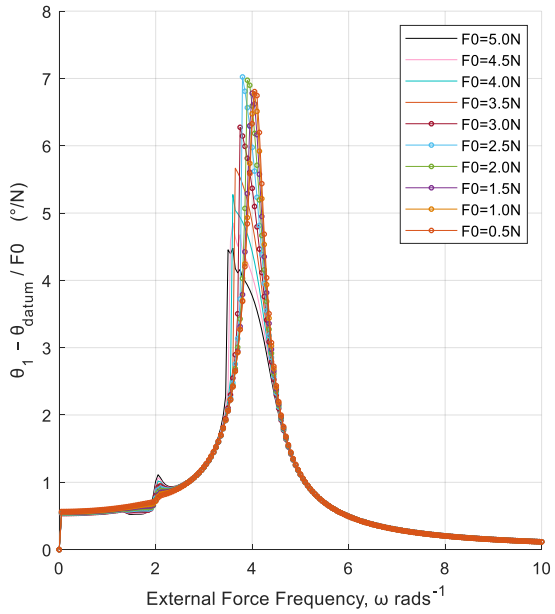

Figure 9: Normalized Frequency Response (FR's) of the Overcentre Mechanism from Figure 8. Damping coefficient: 1 Nsm^{-1}.

3.3 Results

It is clear from results in Figure 6 that nonlinearity is present within the system. The appearance of a hysteresis loop is indicative of the system's bi-stability, with the mechanism's steady state responses able to switch between the upper and lower branch solutions depending upon whether the applied external force surpasses the respective limit points.

Figures 7a) and b) show the dynamic response of the baseline Overcentre Mechanism under free and forced excitation both starting with θ_1=45° at time t=0. For the forced excitation case, a sinusoidal force in the form F=F0sin(ωt) was considered to mimic harmonic vibration loads and applied vertically at the bar connections as in Figure 4. Two forcing cases were considered, one with a forcing amplitude of 3N and the other with forcing amplitude 10N. The value of forcing frequency applied for both was 1.5 $rads^{-1}$. Figure 7b) illustrates the nonlinear nature of the Overcentre Mechanism, with responses attracted to either 'upper' limit cycle solutions (θ_1>0) or 'lower' limit cycle solutions (θ_1<0) depending upon the magnitude of forcing amplitude applied, indicative of the bi-stable nature of the mechanism. In the cases presented in Figure 7b), upper limit cycle solutions are obtained when F0=3N and lower limit cycle solutions are obtained when F0=10N.

Figure 7b) also provides further demonstration of the capabilities of the Udwadia-Kalaba scheme to accurately model non-linear systems. The strong agreement in Figures 7a) and b) between the three modelling approaches verifies the formulations of the dynamic equations used within the Udwadia-Kalaba modelling approach.

Similar investigative studies were also conducted on the configurations of the overcentre mechanism that deviated from geometric symmetry. Throughout, strong agreement was observed between the dynamic responses provided from models derived through the Udwadia-Kalaba approach, the Lagrangian approach and MATLAB MBD toolkit Simscape. Similar to previous studies [13, 14, 15], the results demonstrate the capability of the Udwadia-Kalaba scheme to model a generic multi-body system subjected to kinematical constraints.

An FR analysis was conducted on the baseline Overcentre Mechanism to identify the location of its theoretical resonance frequency due to the parallels and wider purpose of exploring the natural frequencies of the candidate inceptor system.

The FR's in Figure 8 generated from the Lagrangian reduced order model of the Overcentre Mechanism suggest the systems resonant frequency location lies in the region of 4 $rads^{-1}$. A separate eigenvalue analysis of the linearized version of this reduced order state model predicted a single natural frequency of 4.083 $rads^{-1}$. Findings from Figure 8 also demonstrate the nonlinear nature of the overcentre mechanism in addition to the conclusions arrived at from the static analysis investigation in Figure 6. In Figure 8, the nonlinear softening effect is observed as system resonant frequency peak locations reduce with increasing external forcing amplitudes. Further evidence of nonlinearity is seen with the heights of the system resonance peaks which do not scale in a linear manner with external forcing amplitudes which may be observed from the normalized FR plots in Figure 9. The presence of sub harmonic peaks in the forcing frequency region of 2 $rads^{-1}$, approximately half of the system's resonant frequency can also be attributed to the systems non-linear behaviour property.

Dynamic analysis of the presented Overcentre Mechanism has demonstrated the applicability of the Udwadia-Kabala dynamic modelling approach for multibody systems subjected to kinematical constraints. This approach is now proposed for the dynamic modelling of the inceptor to explore its dynamic characteristics.

Presented at 45th European Rotorcraft Forum, Warsaw, Poland, 17-20 September, 2019

4. THE CANDIDATE INCEPTOR

The candidate inceptor is an active collective stick unit. Helicopter collective sticks govern the pitch angle of main rotor blades collectively, thereby dictating the vertical lift generated. Figure 10a) is an example of a collective stick inceptor. However this work will only consider the modelling of the inceptor mechanism within the chassis as opposed to complete system unit. A MATLAB Simscape representation of the kinematical behaviour of the inceptor mechanism is presented in Figure 11.

a)

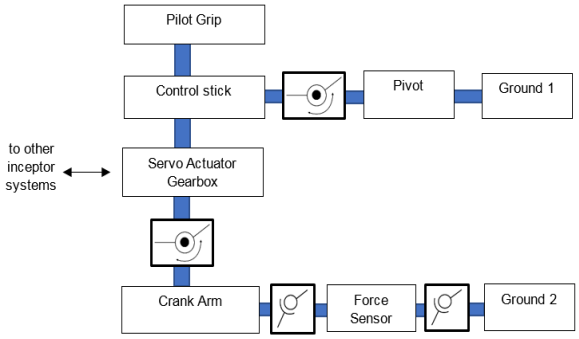

b)

Figure 10: Collective stick inceptor a) Example collective stick inceptor system[18] b) functional block diagram schematic of inceptor central components.

The inceptor mechanism components of interest include the control stick, seen protruding out of the inceptor chassis in Figure 10a). In addition, a servo actuator gearbox is connected to the control stick via a rotating shaft element that is also rigidly connected to a crank arm link. In Figure 11, the control stick is represented by the yellow-green-red link connection whilst the crank arm is represented through the cyan link. The end of this crank arm is connected to a force sensor element represented as the orange link which is fixed in position at its other end.

The application of the Udwadia-Kalaba modelling scheme to the inceptor mechanism poses unique challenges due to the 3D mechanical nature of the inceptor mechanism with multiple components rotating out of plane. Whilst the control stick may rotate in the Y-X plane through an angle φ as seen in Figure 11a), the crank arm which is also connected to the servo actuator gearbox shaft, rotates in its local Y-Z plane through an angle δ shown in Figure 11b).

4.1 Inceptor Mechanism Static Model

The inceptor mechanism was discretized into a series of individual bodies deemed of interest and geometric constraint equations governing the kinematic behaviour of each body derived in similar fashion to those for the Overcentre Mechanism outlined in Section 3.

A brief summary of the processes involved in deriving the geometric constraint equations of each body of the inceptor mechanism is presented.

The system of geometric constraint equations governing the positions of individual bodies were constructed by firstly defining the Centre of Gravity (CG) positions of each body with respect to their local co-ordinate system frame.

$P_{Body1}^{\ Frame}$: CG position of Body 1 in the frame of reference denoted 'Frame'

Matrix Transformations are then successively applied to obtain the position of the body CG in the Global reference frame. A generic outline is presented in Eq.14.

$$(14)\quad P_{Body1}^{\ Global} = [\ (R_i) * P_{Body1}^{\ local}\ ] + T$$

$$(15)\quad P_{Body1}^{\ Global} = \begin{bmatrix} X_{CG} \\ Y_{CG} \\ Z_{CG} \end{bmatrix} \qquad (16)\quad P_{Body1}^{\ local} = \begin{bmatrix} x_{CG} \\ y_{CG} \\ z_{CG} \end{bmatrix}$$

R_i denotes a rotation transformation with respect to a specific axis as in Eqs. (17) to (19). T denotes a Translational transformation.

$$(17)\quad R_X = \begin{bmatrix} 1 & 0 & 0 \\ 0 & \cos(\delta) & \sin(\delta) \\ 0 & -\sin(\delta) & \cos(\delta) \end{bmatrix}$$

Presented at 45th European Rotorcraft Forum, Warsaw, Poland, 17-20 September, 2019

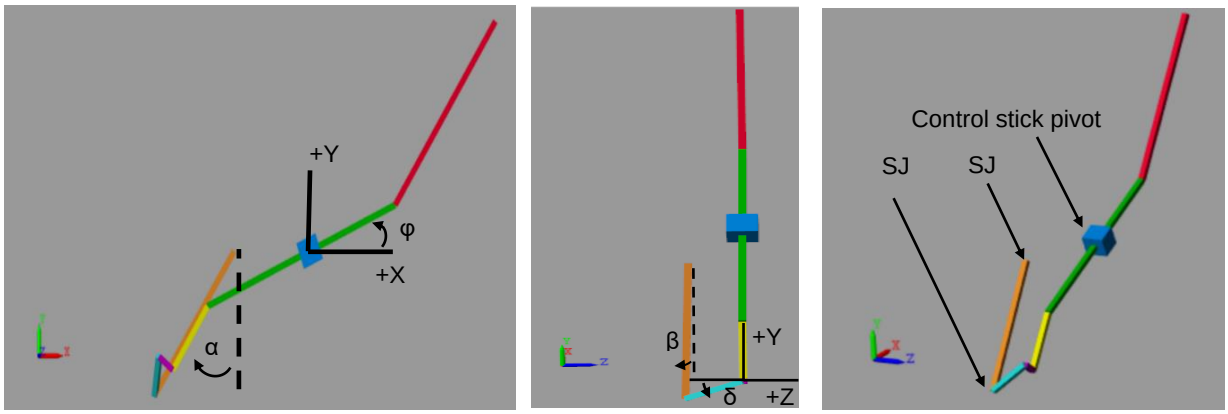

a) b) c)

Figure 11: MATLAB Simscape kinematical model of the collective stick inceptor. SJ denotes a Spherical Joint.

$$(18)\ R_Y = \begin{bmatrix} \cos(\theta) & 0 & -\sin(\theta) \\ 0 & 1 & 0 \\ \sin(\theta) & 0 & \cos(\theta) \end{bmatrix}$$

$$(19)\ R_Z = \begin{bmatrix} \cos(\alpha) & \sin(\alpha) & 0 \\ -\sin(\alpha) & \cos(\alpha) & 0 \\ 0 & 0 & 1 \end{bmatrix}$$

The static response of the inceptor mechanism associated with the derived constraint equations was firstly modelled and solved through the MATLAB FSOLVE function. The control stick angle φ was selected as the user-varied parameter and the ratio of variation of control stick angle φ with servo actuator shaft rotation δ represents the quantity to be investigated for static analysis.

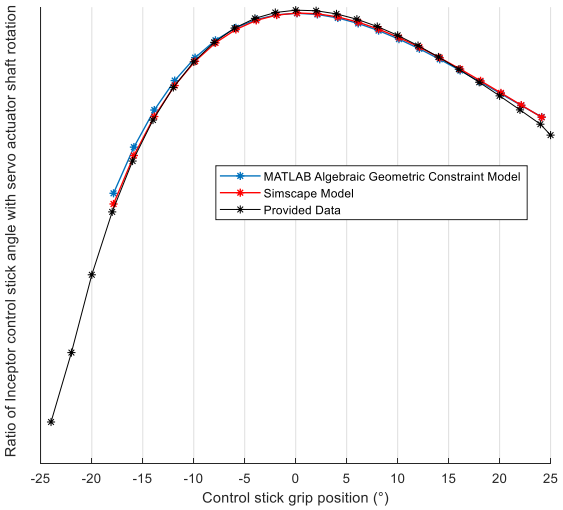

Figure 12: Inceptor static response when control stick angle φ varied.

Static analysis was also conducted on an additional MATLAB Simscape inceptor mechanism model and results from both methods cross compared with baseline provided data for validation

Figure 12 shows that Inceptor static responses obtained from the system of derived algebraic geometric constraint equations and Simscape MBD model showed close agreement with the provided inceptor data. The very slight variations were assumed to be due to the assumed geometry simplifications and definitions in adopted parameter values, complications arose in attempting to attain exact matching between the algebraic constraint model and Simscape MBD model with provided data.

It is clear from the behaviour of variables considered in the static analysis that the inceptor system is non-linear, with clear disproportionate variations in the ratio of control stick angle and servo actuator shaft rotations.

Results from Figure 12 suggest operating in the control stick range 0° ± 5° would provide the subject pilot with optimal collective stick control due to the maxima of ratios between applied control stick angle and servo actuator shaft rotations. A systematic offset exists between angular definitions relating to the control stick angle from the horizontal.

Presented at 45th European Rotorcraft Forum, Warsaw, Poland, 17-20 September, 2019

4.2 Inceptor Mechanism Dynamic Model

Dynamic modelling of the inceptor mechanism using the Udwadia-Kalaba approach was conducted upon validating the derived geometric constraint equations with provided data. This dynamic model was then used as the basis to conduct a frequency response analysis to determine the inceptor mechanism's resonant frequencies.

Frequency response analyses were conducted by modelling the application of an externally applied displacement base excitation to the inceptor mechanism to mimic excitation via a translational shaker table. The external displacement was modelled as a sinusoidal waveform with point of application at the control stick rotational pivot point deemed the initial ground datum position. This ground pivot is illustrated in Figure 11 by the solid blue block.

The sinusoidal displacement applied at the inceptor control stick rotational pivot point is in the form $D=D0\sin(\omega t)$ with D representing the applied displacement (mm) in the horizontal axis, D0 the displacement amplitude (mm) and ω the applied displacement frequency (rads^{-1}). Damping in the form of a rotary damper was modelled at the rotating shaft element located at the end of the inceptor's servo actuator gearbox.

Within the Udwadia-Kalaba dynamic formulations, this horizontal sinusoidal displacement was embedded within the geometric constraint equations associated with horizontal translational states.

23 positional and angular orientation states describing the inceptor mechanism were identified and 21 constraint equations formulated. Theoretically, two resonant frequency peaks are expected from the outcomes of frequency response analyses, implying the inceptor mechanism as effectively a 2-DoF system.

Time simulations of increasing external displacement frequency levels were initially performed using coarse frequency increments of 1 rads^{-1} to provide early indications of the inceptor mechanism's possible resonance frequency locations. Additional time simulations were then performed using refined frequency step increments of 0.1 rads^{-1} in the frequency regions identified as likely containing the inceptor mechanism's resonant frequencies in order to further explore the inceptor mechanism's dynamic behaviour. The maxima of response solutions within the settled state response regions were then extracted for the FR analysis. Figure 13 is a time history of the dynamic behaviour of the inceptor mechanism control stick angle φ under the influence of the applied horizontal sinusoidal displacement and illustrates the process involving coarse and refined displacement frequency increment levels to build an insight into the inceptor mechanism's dynamic response. The value of base-excitation displacement amplitude presented in Figure 13 is 7mm and responses in red were obtained from time simulations that used a coarse frequency step increment of 1 rads^{-1}. Responses in blue were obtained from time simulations that used the refined frequency step increment of 0.1 rads^{-1}. The fine vertical response limits observed in Figure 13 represent transient responses as system initial conditions are re-

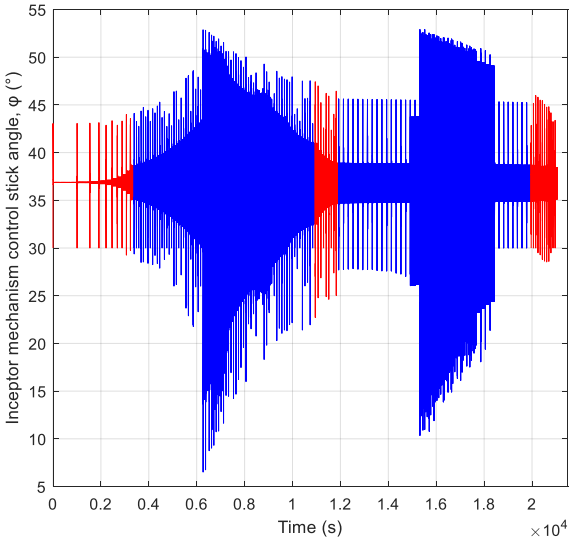

Figure 13: Time history simulation of the inceptor mechanism control stick angle φ (°). D0 = 7mm. Damping coefficient: 50 lbfs-inch/rad.

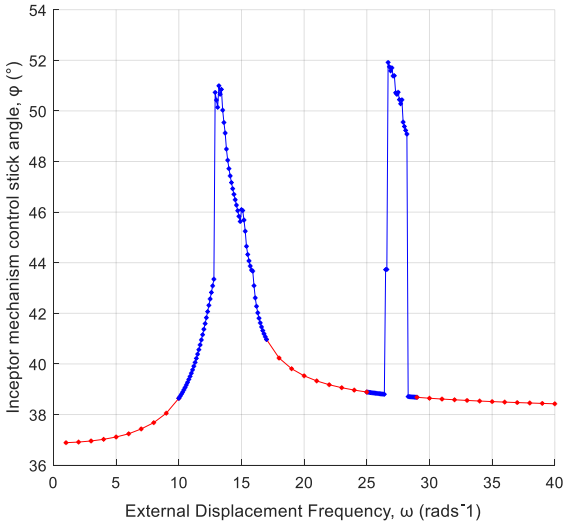

Figure 14: Frequency response of the inceptor mechanism control stick angle φ (°). D0 = 7mm. Damping coefficient: 50 lbfs-inch/rad.

Presented at 45th European Rotorcraft Forum, Warsaw, Poland, 17-20 September, 2019

initialised every displacement frequency increment. Figure 14 is the corresponding frequency response spectrum of the inceptor mechanism's control stick angle time response behaviour from Figure 13.

The time duration simulated at each displacement frequency level was determined based on specifying a target value for the number of oscillation cycles associated with the applied sinusoidal displacement to achieve steady periodic response behaviours prior to a frequency step increment

From Figure 14, resonance is observed at displacement frequency levels of 13.2 rads^{-1} and 26.7 rads^{-1}. However, the second resonance peak indicates the presence of a level of nonlinearity in the sense that this peak is not well defined as in linear cases. Evidence of nonlinearity may also be seen through the inceptor mechanism's frequency responses through the sharp increases in frequency resonance responses prior to gradual decreases as seen in Figure 14. These observations are more notably so at the mechanism's first resonance frequency peak, alluding to complex behaviours.

The amplitude of the applied displacement excitation (D0) was reduced to investigate whether it influences the complex nonlinear behaviour observed in the regions of the mechanism's resonance frequencies. In Figure 15, the amplitude of the applied displacement excitation (D0) was reduced from 7mm to 5mm.

Observations from Figure 15 suggest that when the amplitude of the applied displacement excitation is reduced to 5mm, the first resonance peak remains comparable with that of D0=7mm. Resonance is still observed at displacement frequency level 13.2 rads^{-1}. However, the appearance of the mechanism's second resonance frequency peak drastically alters. Reducing the displacement excitation amplitude to 5mm appears to have significantly reduced the magnitude of the second resonance peak, whilst additionally increasing this observed resonance frequency by about 3% to 27.5 rads^{-1}. These observations further illustrate complex nonlinear dynamics of the inceptor model. The effect of nonlinearity is not discussed further in this paper for conciseness. Therefore, the following section detailing sensitivity analyses will continue to assume the displacement excitation amplitude case of 7mm.

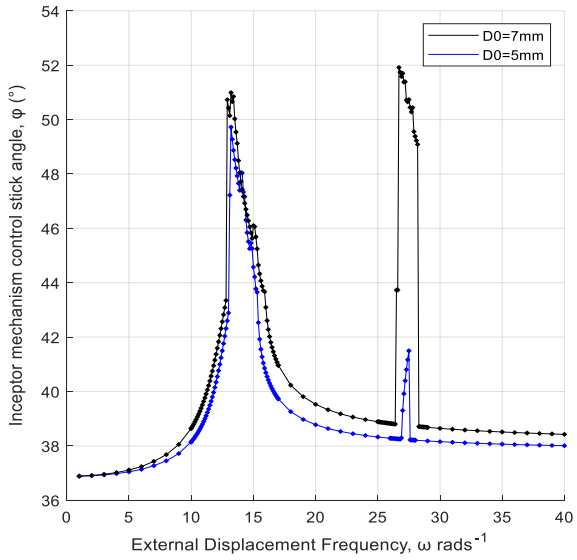

Figure 15: FR comparison of the baseline inceptor mechanism between displacement excitation amplitude (D0) cases of 7mm and 5mm. Damping coefficient: 50 lbfs-inch/rad.

4.2.1 Sensitivity Analyses

Sensitivity studies were conducted on the inceptor mechanism model formulated from the Udwadia-Kalaba scheme for the external displacement excitation amplitude case considered, D0 7mm.

The intention of conducting sensitivity analysis for this work is to demonstrate that altering inceptor design parameters may influence resonant frequencies. The results would give insight into how these parameters can be tuned to move resonant frequencies away from baseline nominal values.

Consequently, only two inceptor design parameters were considered for sensitivity studies, outlined below:

- Force sensor stiffness : ±10%
- Servo actuator gearbox mass: ±5%

The servo actuator gearbox was considered due to its highest weight contribution within the inceptor mechanism. Individual masses of bodies within the inceptor mechanism are typically fixed, however a modest value of +5% to the servo actuator gearbox mass was investigated to account for the influence of cabling connections to the gearbox. -5% of the servo actuator gearbox mass was also considered as part of the parametric study. Limits of ±10% were considered for the force sensor element stiffness based on advice.

The influence of lengths and distances between individual inceptor mechanism component bodies were not considered due to their influence on the mechanism's static response behaviour (Figure 12).

The baseline inceptor mechanism is identified as having two distinct resonance frequencies located at 13.2 rads^{-1} and 26.7 rads^{-1} as presented in Tables 2

Presented at 45th European Rotorcraft Forum, Warsaw, Poland, 17-20 September, 2019

and 3 for the displacement excitation amplitude case of 7mm. This value reflects a representative value of a shaker table providing base excitation to the collective stick unit system.

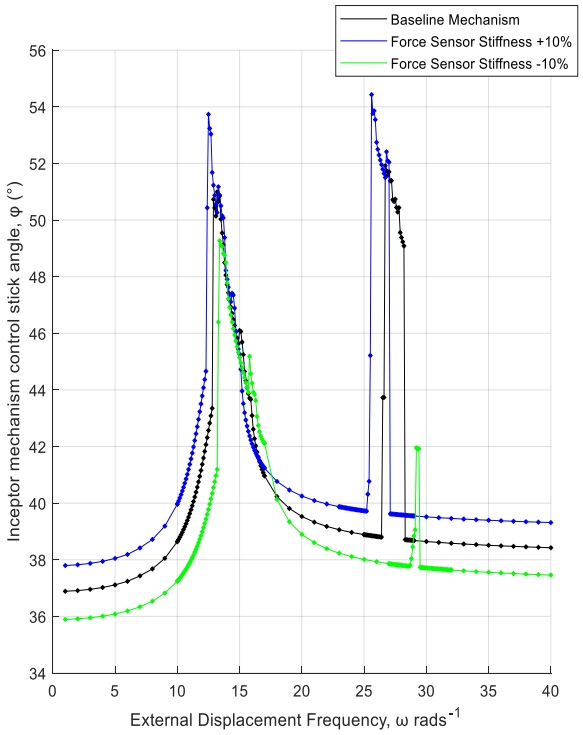

Figure 16: Sensitivity analysis of baseline inceptor mechanism against mechanism with ±10% Force Sensor stiffness. D0: 7mm. Damping coefficient: 50 lbfs-inch/rad.

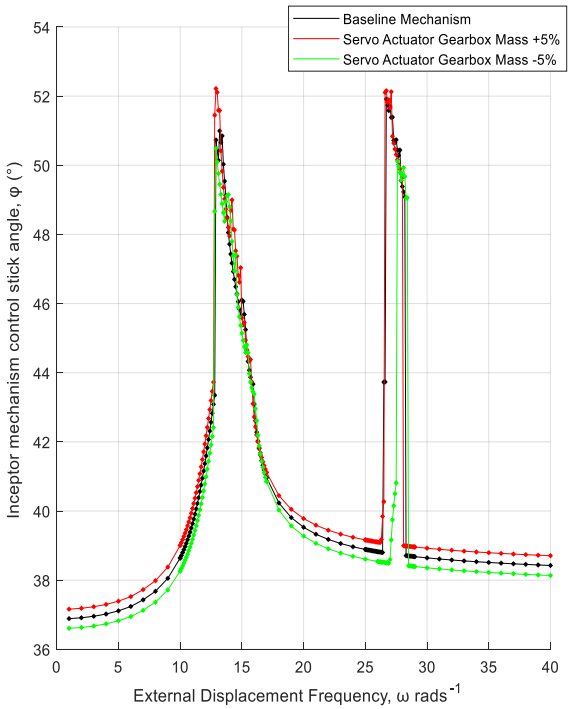

Figure 17: Sensitivity analysis of baseline inceptor mechanism against mechanism with ±5% Servo Actuator Gearbox mass. D0: 7mm. Damping coefficient: 50 lbfs-inch/rad.

Table 2: Sensitivity of the inceptor resonance frequencies with ±10% change in the mechanism's force sensor stiffness. D0=7mm

Sensitivity Study:	**Baseline Mechanism**	**+10% Force sensor stiffness**	**-10% Force sensor stiffness**
First mode	ω =13.2 rads^{-1}	**-5.30%** (ω = 12.5 rads^{-1})	**+1.52%** (ω = 13.4 rads^{-1})
Second mode	ω = 26.7 rads^{-1}	**-4.12%** (ω = 25.6 rads^{-1})	**+9.36%** (ω = 29.2 rads^{-1})

Table 3: Sensitivity of the inceptor resonance frequencies with ±5% change in the mechanism's servo actuator gearbox mass. D0=7mm

Sensitivity Study:	**Baseline Mechanism**	**+5% Servo actuator gearbox mass:**	**-5% Servo actuator gearbox mass:**
First mode	ω = 13.2 rads^{-1}	**-2.27%** (ω = 12.9 rads^{-1})	**-2.27%** (ω = 12.9 rads^{-1})
Second mode	ω = 26.7 rads^{-1}	**0%** (ω = 26.7 rads^{-1})	**+3.37%** (ω = 27.6 rads^{-1})

Presented at 45th European Rotorcraft Forum, Warsaw, Poland, 17-20 September, 2019

Results in Figures 16 and 17 show that the resonance frequency locations of the inceptor mechanism may indeed be influenced through modifications to design parameters.

Varying both the force sensor stiffness and servo actuator gearbox mass is seen to influence the datum settling responses of the inceptor mechanism control stick angle φ, seen through the vertical shifts in frequency response curves. These observations are expected due to alterations in the baseline inceptor mechanism configuration with design parameter modifications.

Tables 2 and 3 present a summary of findings of the observed shifts in the appearances of the inceptor mechanism's resonance frequencies from the conducted parameter studies. Results suggest that varying the force sensor element stiffness by ±10% provides an effective shift of the frequency spectrum either side of the baseline inceptor mechanism frequency spectrum, not accounting for the changes in datum φ orientations. With a +10% increase in the inceptor mechanism's force sensor stiffness, the first and second resonance frequencies are observed to shift by -5.30% and -4.12% respectively whilst a corresponding 10% decrease in force sensor stiffness is seen to provide a +1.52% and +9.36% resonance frequency shift. The unbalanced levels of resonance shifts recorded with modifications to force sensor stiffness coupled with the extent to which the mechanism's second resonance frequency magnitude compressed with the 10% reduction in force sensor stiffness further demonstrates the nonlinear nature of the inceptor mechanism.

The results in Table 3 for the study of varying the inceptor servo actuator gearbox mass by ±5% appears to suggest that the addition of a 5% servo actuator gearbox mass does not influence the mechanism's second resonant frequency which is recorded to remain at the baseline mechanism's value of 26.7 $rads^{-1}$. The mechanism's first resonance frequency is observed to reduce by 2.27% relative to baseline values, however observations from Figure 17 and results in Table 3 suggests this 2.27% reduction in first resonance frequency may also be achieved with a 5% reduction in servo actuator gearbox mass. A +3.37% increase in the mechanism's second resonance frequency is observed with a 5% decrease in servo actuator gearbox mass.

Overall results presented in Tables 2 and 3 show that the resonance frequency locations of the inceptor mechanism may indeed be influenced through modifications to design parameters. The observed variations in datum orientations of the control stick angle φ with parameter modification are expected due to alterations in the baseline inceptor mechanism configuration.

5. CONCLUSIONS

This paper explores the dynamic modelling methodology formulated by Udwadia-Kalaba and its application to a candidate inceptor mechanism, and a case study model was illustrated. Dynamic analysis of the initially presented case study model, the Overcentre Mechanism, demonstrated the applicability of the Udwadia-Kabala dynamic modelling approach for multibody systems subjected to kinematical constraints that also display nonlinear behaviour.

Static modelling of the sample inceptor mechanism system has provided means of validation for the derived geometric constraint equations.

For the candidate inceptor, dynamic analysis of the inceptor mechanism system using the Udwadia-Kalaba scheme adequately predicted the presence and locations of the mechanism's resonance frequencies.

Additionally, sensitivity analysis investigations on inceptor mechanism design parameters demonstrated that system resonance frequencies may be influenced and tuned away from nominal baseline values.

The development of an efficiently configurable mathematical model of an active inceptor would provide an early low-cost means of predicting inceptor mechanism dynamics in the preliminary design stage. Adverse vibration issues may be pre-empted through frequency response analyses and acceptable design configurations identified that comply with specified frequency restrictions through sensitivity study investigations on system design parameters.

Future research efforts will focus on incorporating flexibility of elements within the inceptor mechanism, experimental testing for cross comparison and validation, and implementing numerical continuation methods for computational efficiencies. Additional work will be directed at investigating the observed nonlinearity presented in this work.

6. ACKNOWLEDGEMENT

The research presented in this paper is funded by EPSRC and BAE Systems Plc through an Industrial CASE award (no. 17000065).

Presented at 45th European Rotorcraft Forum, Warsaw, Poland, 17-20 September, 2019

7. REFERENCES

[1]: Anon. *Active Inceptor Systems,* BAE Systems Plc. http://www.baesystems-ps.com/pdf/ais_mil_brochure.pdf, accessed Aug.,2018.

[2]: Anon. *Air France flight AF 447 Rio de Janeiro-Paris Final Report*, 2012, BEA, https://www.bea.aero/docspa/2009/f-cp090601.en/pdf/f-cp090601.en.pdf

[3]: C.A. Malpica, W. von Grunhagen*, In Flight Evaluation of Active Inceptor Force-Feel Characteristics and Handling Qualities.* Fort Worth, United States. Presented at the American Helicopter Society 68th Annual Forum, May, 2012.

[4]: G. Quaranta, P. Masarati, J.Venrooij, *Impact of pilots' biodynamic feedthrough on rotorcraft by robust stability*. Elsevier Science Ltd, Journal of Sound and Vibration 2013;332:4948-4962.

[5]: M. D. Pavel, M. Jump, P.Masarati, L. Zaichik, B. Dang-Vu, H.Smaili, G.Quaranta, O. Stroosma, D.Yilmaz, M.Johnes, M.Gennaretti, A.Ionita, *Practises to identify and prevent adverse aircraft-and-rotorcraft-pilot couplings- A ground simulator perspective.* Elsevier Science Ltd, Progress in Aerospace Sciences 2015;77:54-87.

[6]: M.D.Pavel, M.Jump, B.D-Vu, P.Masarati, M.Gennaretti, A.Ionita, L.Zaichik, H.Smaili, G.Quaranta, D.Yilmaz, M.Jones, J.Serafini, J.Malecki, *Adverse rotorcraft pilot couplings-Past, present and future challenges.* Elsevier Science Ltd, Progress in Aerospace Sciences 2013;62:1-51.

[7]: Anon. *Pilot controls- active sticks*, BAESystems, http://www.baesystems-ps.com/pilot-controls.php, accessed Feb.,2019.

[8]: Anon. *Aerospace Active Inceptor Systems for Aircraft Flight and Engine Controls,* Aerospace Recommended Practice (ARP) 5764, SAE International, 2013.

[9]: Military Standard (MIL STD)- 810G, *Transportation Tailoring Guidance for Vibration Exposure Definition,* Method 514.6, Annex C, 317-318, 2008.

[10]: F.E. Udwadia, R.E. Kalaba, *Analytical Dynamics A New Approach;* Cambridge University Press: Cambridge,1996.

[11]: Udwadia, Phohomsiri,Explicit *Poincaré equations of motion for general constrained systems. Part I. Analytical results* 463 *Proceedings of the Royal Society A: Mathematical, Physical and Engineering Science,* 2007.

[12]: Moore-Penrose pseudoinverse documentation, MathWorks, https://www.mathworks.com/help/matlab/ref/pinv.html

[13]: M.C. Nielson, O.A. Eidsvik, M. Blanke, I. Schjolberg, *Validation of Multi-Body Modelling Methodology for Reconfigurable Underwater Robots.* Presented in the OCEANS 2016 MTS/IEEE Monterey conference, IEEE, Sept, 2016.

[14]: C. Li, H. Zhao, S. Zhen, H. Sun, K. Shao, *Udwadia-Kalaba theory for the control of bulldozer link lever*. Advances in Mechanical Engineering, 2018.

[15]: E. Pennestri, P. P. Valentini, D. de Falco, *An application of the Udwadia-Kalaba dynamic formulation to flexible multibody systems,* Journal of the Franklin Institute, Vol 347, Issue 1, 173-194, 2010.

[16]: J. Knowles, *Continuation Analysis of Landing Gear Mechanisms*, PhD thesis, University of Bristol, 2012.

[17]: Simscape documentation, MathWorks, https://uk.mathworks.com/products/simscape.html

[18]: Anon. *Active controls,* Stirling Dynamics - https://www.stirling-dynamics.com/products/active-controls

Presented at 45th European Rotorcraft Forum, Warsaw, Poland, 17-20 September, 2019